Acta Pharmaceutica Sinica B 2025;15(5):2529–2544

Chinese Pharmaceutical Association
Institute of Materia Medica, Chinese Academy of Medical Sciences

Acta Pharmaceutica Sinica B

www.elsevier.com/locate/apsb
www.sciencedirect.com

ORIGINAL ARTICLE

Targeting the JAK2–STAT3–UCHL3–ENO1 axis suppresses glycolysis and enhances the sensitivity to 5-FU chemotherapy in *TP53*-mutant colorectal cancer

Haisong Xin[a,b,c,†], Zitong Zhao[b,†], Shichao Guo[b], Ruoxi Tian[d], Liying Ma[b], Yang Yang[f], Lianmei Zhao[g], Guanglin Wang[e], Baokun Li[e], Xuhua Hu[e], Yongmei Song[b,*], Guiying Wang[a,c,e,*]

[a]*Department of General Surgery, the Second Hospital of Hebei Medical University, Shijiazhuang 050000, China*
[b]*State Key Laboratory of Molecular Oncology, National Cancer Center/National Clinical Research Center for Cancer/Cancer Hospital, Chinese Academy of Medical Sciences and Peking Union Medical College, Beijing 100021, China*
[c]*Hebei Key Laboratory of Etiology Tracing and Individualized Diagnosis and Treatment for Digestive System Carcinoma, the Second Hospital of Hebei Medical University, Shijiazhuang 050000, China*
[d]*Department of Colorectal Surgery, National Cancer Center/National Clinical Research Center for Cancer/Cancer Hospital, Chinese Academy of Medical Sciences and Peking Union Medical College, Beijing 100021, China*
[e]*The Second Department of General Surgery, the Fourth Hospital of Hebei Medical University, Shijiazhuang 050011, China*
[f]*Department of General Surgery, the Third Hospital of Hebei Medical University, Shijiazhuang 050051, China*
[g]*Research Center, the Fourth Hospital of Hebei Medical University, Shijiazhuang 050011, China*

Received 19 June 2024; received in revised form 15 September 2024; accepted 20 December 2024

KEY WORDS

Colorectal cancer;
TP53 mutation;
UCHL3;
Glycolysis;
Stem-like properties;

Abstract Approximately 60% of colorectal cancer (CRC) patients exhibit *TP53* mutations, which are strongly associated with tumor progression, chemotherapy resistance, and an unfavorable prognosis. However, targeting p53 has historically been challenging, and currently, there are no approved p53-based therapeutics for clinical use worldwide. In this study, we discovered that ubiquitin carboxyl terminal hydrolase L3 (UCHL3) plays a crucial role in high-level glycolysis, enhanced stem-like properties, and 5-fluorouracil (5-FU) chemoresistance in *TP53*-mutant CRC by exerting its deubiquitinating enzyme

*Corresponding authors.
E-mail addresses: symlh2006@163.com (Yongmei Song), wangguiying@hebmu.edu.cn (Guiying Wang).
[†]These authors made equal contributions to this work.

Peer review under the responsibility of Chinese Pharmaceutical Association and Institute of Materia Medica, Chinese Academy of Medical Sciences.

https://doi.org/10.1016/j.apsb.2025.03.041

Chemotherapy resistance; JAK2−STAT3 pathway; Pacritinib

activity to stabilize α-enolase (ENO1) protein. Notably, we identified a newly Food and Drug Administration (FDA)-approved drug, pacritinib, that potently suppresses UCHL3 expression by blocking the janus kinase 2 (JAK2)−signal transducer and activator of transcription 3 (STAT3) pathway in *TP*53-mutant CRC. Furthermore, Pacritinib was demonstrated to effectively inhibit glycolysis and improve the sensitivity to 5-FU chemotherapy in *TP53*-mutant CRC. Our findings suggest that targeting the JAK2−STAT3 −UCHL3−ENO1 axis is a promising strategy to suppress glycolysis and enhance the efficacy of 5-FU chemotherapy in *TP53*-mutant CRC. Pacritinib shows potential for clinical application in the treatment of *TP53*-mutant CRC.

1. Introduction

Colorectal cancer (CRC) ranks as the third most common and fourth deadliest cancer globally, causing nearly 900,000 deaths annually[1]. The acquisition of multiple tumor-associated mutations drives the development and malignant progression of CRC. Comprehensive genome analyses have revealed that *TP53* mutations occur in approximately 60% of CRC patients, with the incidence increasing to 80% in stage IV CRC patients with distant metastases[2]. *TP53* mutation is associated with tumor progression, chemoresistance, and an unfavorable prognosis in various types of cancers, including CRC[3].

TP53, a well-known tumor suppressor gene, is often referred to as the 'guardian of the genome'. In response to various cellular stresses, p53 is activated and then orchestrates a series of biological processes, including cell cycle arrest, apoptosis, and senescence, thereby inhibiting tumorigenesis and enhancing chemosensitivity[4-6]. Moreover, p53 directly influences various metabolic pathways, including the inhibition of glycolysis, enabling cancer cells to respond to metabolic stress[7,8]. When *TP53* is mutated, in addition to losing the caner−inhibitory activities of wild-type p53 (wtp53), some p53 mutants (mutp53) also acquire new gain-of-function (GOF) activities that further promote cancer[9]. *TP53* mutation has been reported to enhance glycolysis by increasing the translocation of glucose transporter 1 to the plasma membrane and promoting the expression of hexokinase 2, a key enzyme in glycolytic[10,11]. Additionally, *TP53* mutation confers chemoresistance on cancer cells by enhancing drug efflux and inactivation, promoting DNA repair, attenuating apoptosis, and impairing autophagy[12-14]. Moreover, the inactivation or mutation of wtp53 promotes the malignant transformation of stem cells and favors the formation of cancer stem cells (CSCs), thereby enhancing the stem-like properties and chemoresistance of cancer cells[15-17]. In recent decades, restoring p53 functionality has been an attractive strategy for developing novel anticancer drugs[18]. Unfortunately, p53, as a nuclear transcription factor, lacks typical drug target features, leading to very few drug development programs reaching the late stages of clinical trials[19]. Therefore, it is essential to investigate the specific mechanisms of *TP53* mutation that leads to a high level of glycolysis, enhanced stem-like properties, and chemoresistance in order to identify new therapeutic targets and improve the prognosis for CRC patients with *TP53* mutations (Fig. 1A).

Ubiquitin carboxyl terminal hydrolase L3 (UCHL3) belongs to the family of ubiquitin C-terminal hydrolases (UCHs), which is a subfamily of deubiquitinating enzymes (DUBs) consisting of four members: UCHL1, UCHL3, UCHL5/UCH37, and BRCA1 associated protein-1 (BAP1). With only a conserved catalytic domain (UCH domain) composed of 230 amino acids, UCHL3 exerts its deubiquitinating enzyme activity by cleaving polyubiquitin chains from substrate proteins[20]. Recent studies have revealed UCHL3 is highly expressed in several types of cancer and plays a crucial role in cell cycle regulation, DNA damage repair, radiotherapy and chemotherapy resistance, and malignant progression[21-26]. However, the precious role and underlying mechanism of UCHL3 in high-level glycolysis, enhanced stem-like properties, and 5-fluorouracil (5-FU) chemoresistance of *TP53*-mutant CRC remain elusive. Additionally, pacritinib is an orally administered small molecule inhibitor targeting janus kinase 2 (JAK2) and interleukin-1 receptor associated kinase 1 (IRAK1) that was approved by the Food and Drug Administration (FDA) in February 2022 for treating myelofibrosis in the United States[27]. However, there have been no reports on the impact of pacritinib on glycolysis or chemotherapy sensitivity to 5-FU in CRC with *TP53* mutation.

In this study, we have uncovered the crucial role of UCHL3 in high-level glycolysis, enhanced stem-like properties, and 5-FU chemoresistance in *TP53*-mutant CRC. Notably, through screening an FDA-approved drug library with the expectation to repurpose existing drugs to treat *TP53*-mutant CRC, we have identified that Pacritinib effectively reverses high-level glycolysis and enhances the sensitivity of 5-FU chemotherapy in *TP53*-mutant CRC by blocking the JAK2-signal transducer and activator of transcription 3 (STAT3)−UCHL3−α-Enolase (ENO1) axis. This provides a promising therapeutic strategy for improving the prognosis of CRC patients with *TP53* mutations.

2. Materials and methods

A detailed description of the Materials and Methods for Cell Culture and Transfection, Plasmids, siRNAs, Antibodies, and Chemicals, Immunohistochemistry (IHC), Glycolysis Rate Measurement, Metabolite Labeling and Measurement by Gas Chromatography−Mass Spectrometry (GC−MS), Lentiviral Infection, Spheroid Formation Assay, Flow Cytometry Analysis, Half Maximal Inhibitory Concentration (IC_{50}) Analysis, Cell Apoptosis Assay, Cell Proliferation Assay, Transwell Assay, and Clone Formation Assay, Coimmunoprecipitation (Co-IP) and Western Blotting (WB), Liquid Chromatography−tandem Mass Spectrometry (LC−MS/MS), RNA Extraction and Quantitative Real-time PCR, Chromatin Immunoprecipitation (ChIP) Assay, Dual Luciferase Assay, Bioinformatic Analysis can be found in the Supporting Information for Materials and Methods, as well as in Supporting Information Tables S1−S3.

2.1. Animal experiments

The animal studies were conducted in accordance with national policies for animal health and welfare, and the protocol was approved by the Institutional Animal Care and Use Committee of the Second Hospital of Hebei Medical University (2023-AE098). Male BALB/c nude and NOD/SCID mice (aged 4−5 weeks) were purchased from Beijing Vital River Laboratory Animal Technology Company. The tumor dimensions were measured using Vernier calipers, and tumor volume (V) was calculated according to Eq. (1):

$$V = \text{Width}^2 \times \text{Length} \times 0.537 \quad (1)$$

The maximum tumor diameter permitted by the ethics committee is 1.5 cm, and all of the mouse-loaded tumors in this study did not exceed this limitation. CO_2 inhalation was used as the method for euthanizing mice. CO_2 with over 99% purity was administered into the euthanasia cages at a controlled rate, rendering the mice unconscious within 3 min and minimizing their suffering as much as possible. Pulmonary hemorrhage and other symptoms affecting animal welfare were not observed during the euthanasia process (Supporting Information Fig. S1).

For the *in vivo* stem cell tumorigenesis assay, tumor stem cells were enriched through the spheroid formation assay with SW480 cells (NC, shUCHL3). Gradient numbers of tumor stem cells (5.0×10^3, 1.0×10^4, 5.0×10^4, 1.0×10^5) were subcutaneously injected into the double dorsal flank of NOD/SCID mice, and tumor formation was monitored three times per week. After 45 days, mice were humanely sacrificed *via* CO_2 inhalation, and tumors were harvested for further analysis.

For the subcutaneous tumorigenesis assay in nude mice, 2.5×10^6 SW480 cells (NC, shUCHL3) were subcutaneously injected into the double dorsal flank of BALB/c nude mice, and tumor progression was monitored by tumor volume measurement every four days. The mice were sacrificed by CO_2 inhalation on Day 19, and tumors were harvested and weighed.

For the SW480 cell subcutaneous xenograft tumor model, BALB/c mice were subcutaneously implanted into the left dorsal flank with 2.5×10^6 SW480 cells. When tumors reached a volume of approximately 100 mm^3, mice bearing similar tumor burden were randomly divided into four groups for drug treatment. 5-FU was dissolved in 0.9% normal saline and administered *via* intraperitoneal injection three times per week at a dose of 20 mg/kg. Pacritinib was dissolved in 0.5% carboxymethylcellulose sodium (CMC-Na) and administered orally *via* gavage three times per week at a dose of 100 mg/kg. Tumor volume and body weight were monitored three times per week until the tumor volume reached 2000 mm^3. Mice were euthanized by CO_2 inhalation, and tumors were harvested for future analysis.

For the patient-derived xenograft (PDX) tumor model, PDX tumors with wild-type *TP53* (#CR3424) and *TP53* missense mutation (R273H, R248Q) (#CR14777) were constructed by Crown Bioscience (Suzhou, China). Briefly, tumor tissues were harvested from the tumor-bearing mice of the HuPrime® model and sliced into tumor blocks of 2−3 mm in diameter, which were subcutaneously inoculated in the right anterior scapula of the mice. Upon reaching an average tumor volume of approximately 150 mm^3, the mice were randomly divided into four groups and administered treatment with either the vehicle, 5-FU at a dosage of 20 mg/kg, pacritinib at a dosage of 100 mg/kg, or a combination of both for a total of nine administrations given three times per week. Tumor volume and body weight were monitored three times per week, and mice were euthanized by CO_2 inhalation on Day 28. Subsequently, tumors were collected for further analysis.

2.2. Statistical analysis

Statistical analysis and graphics plotting were performed using IBM SPSS Statistics 21.0 (IBM Crop., Armonk, USA) and GraphPad Prism 7 (Graphpad Software Inc., San Diego, USA). The Wilcoxon rank sum test was utilized to compare IHC staining patterns among different subgroups. The correlation of IHC staining scores was assessed through linear correlation analysis and Kendall's Tau-b test. Survival analysis was conducted using the log-rank test, and the corresponding cumulative survival function curve was plotted *via* the Kaplan−Meier method. Student's *t*-test (2-tailed) was performed to compare differences between the two groups, and data were presented as mean ± standard deviation (SD). $P < 0.05$ was considered statistically significant unless stated otherwise.

3. Results

3.1. UCHL3 is involved in high-level glycolysis caused by TP53 mutation in CRC

To systematically identify DUBs that may be involved in the high-level glycolysis caused by *TP53* mutation in CRC, we adopted a strategy of screening DUBs plasmid library combined with bioinformatic analysis (Fig. 1B). In the initial step, we performed an unbiased screening by individually transfecting 57 DUBs into 293T cells. By setting a cut-off of 1.5-fold upregulation, we identified ubiquitin-specific peptidase 44 (USP44) and UCHL3 as significant inducers of lactate dehydrogenase (LDHA) expression (Fig. 1C, Supporting Information Fig. S2A). Furthermore, in the TCGA database, we found a positive correlation between *USP44* mRNA levels and the PI3K−AKT−mTOR pathway, while *UCHL3* mRNA levels correlated positively with the MYC target genes pathway (Fig. 1D). Activation of these pathways is widely recognized to enhance glycolysis in tumors. Based on these findings, we hypothesized that USP44 and UCHL3 may promote glycolysis in CRC.

The second step involved bioinformatic analysis in the TCGA database, which revealed that *UCHL3* mRNA levels were significantly higher in *TP53* mutant CRC tissues compared to *TP53* wild-type CRC tissues. However, no significant difference was observed in *USP44* expression (Fig. 1E). *TP53* mutation was also found to be more frequent in CRC tissues with high expression of *UCHL3* compared to those with low expression of *UCHL3*, whereas this correlation was not observed with *USP44* (Fig. S2B). Additionally, overexpression of mutant p53 in HCT116 ($TP53^{-/-}$) cells significantly enhanced UCHL3 expression, whereas overexpression of wild-type p53 had the opposite effect. However, USP44 expression remained unaffected (Fig. 1F). Moreover, knockout of wild-type p53 in HCT116 cells led to an increase in UCHL3 expression, while knockdown of mutant p53 in SW480 cells resulted in the opposite effect. Again, no significant change was observed in USP44 expression (Fig. 1G). Next, we performed immunohistochemical analysis of p53 and UCHL3 proteins on a CRC tissue array (Fig. 1H, Fig. S2C). Among the 80 cases, 46 cases (57.5%) exhibited wild-type *TP53*, 23 cases

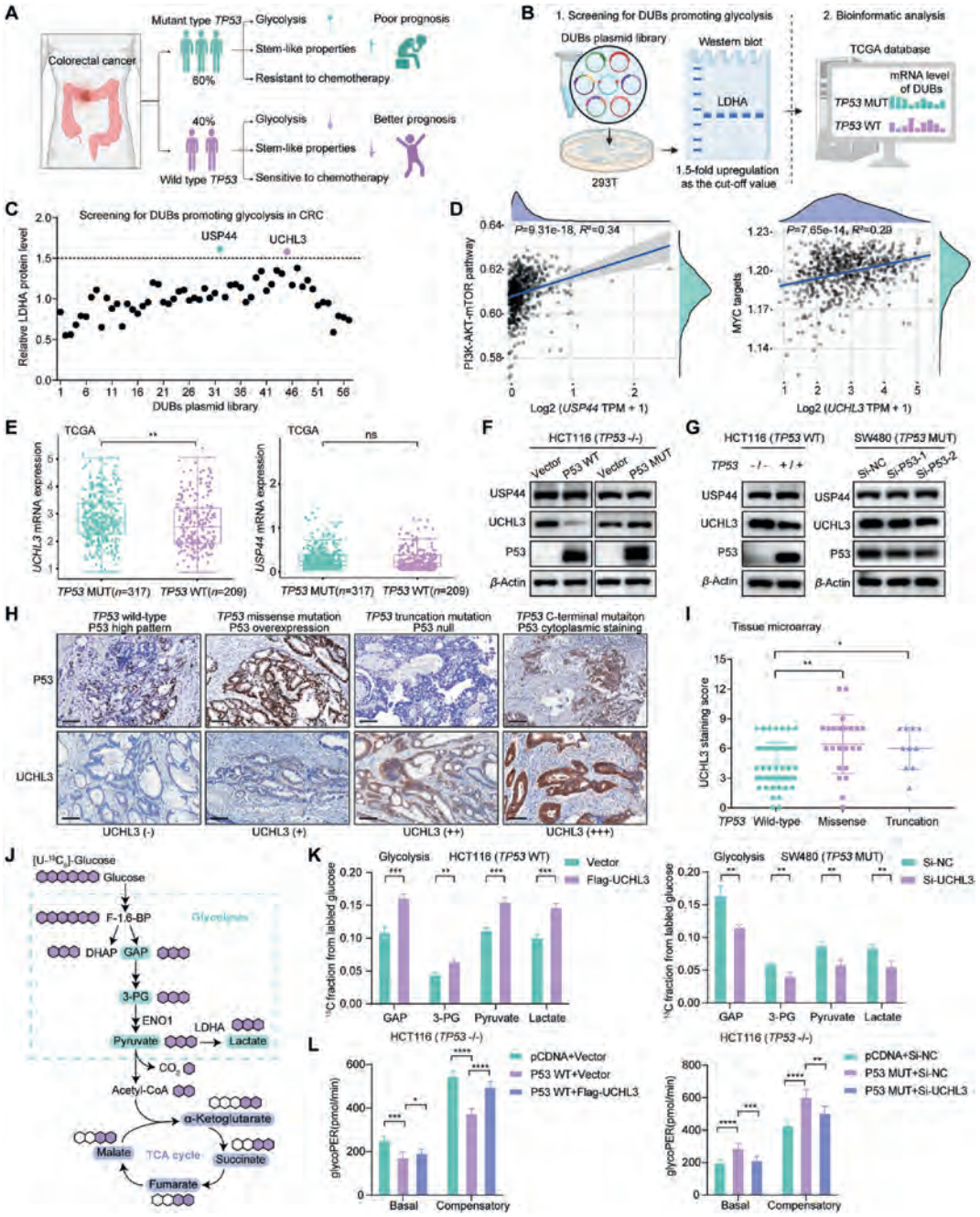

Figure 1 UCHL3 is involved in high-level glycolysis caused by *TP53* mutation in CRC. (A) Our study aimed to identify Deubiquitinating enzymes (DUBs) that contribute to high-level glycolysis, enhanced stem-like properties, and chemotherapy resistance in *TP53*-mutant CRC. (B) Schematic representation of the process for identifying DUBs that may be involved in high-level glycolysis caused by *TP53* mutation in CRC. (C) Quantitative analysis of LDHA protein bands of 293T cells transfected individually with 57 DUBs. (D) Correlations between *USP44*, *UCHL3* expression and glycolysis-related pathways were analyzed in the TCGA database. (E) Comparison of *USP44* and *UCHL3* mRNA levels in *TP53* mutant and wild-type CRC tissues in the TCGA database. (F) Immunoblotting of USP44, UCHL3, and P53 in HCT116 (*TP53*$^{-/-}$) cells transfected with P53 WT and MUT plasmids for 36 h. (G) Immunoblotting of *USP44*, UCHL3, and P53 in HCT116 (*TP53* WT) cells with WT P53 knockout and SW480 (*TP53* MUT) cells with MUT P53 knockdown. (H) Immunohistochemistry (IHC) analyses of P53 and UCHL3 were conducted on a tissue array comprising samples from 80 CRC patients. Representative images of CRC tissues with different staining patterns were shown. Scale bar, 100 μm. (I) Comparison of UCHL3 staining scores in CRC tissues with wild-type and mutant *TP53*. (J) A schematic briefly outlining the landscape of glucose metabolism in mammalian cells. (K) Partial metabolic profiling (glycolysis) of HCT116 (*TP53* WT) and SW480 (*TP53* MUT) cells incubated with uniformly labeled [U−$^{13}C_6$]-glucose. Results from gas chromatography−mass spectrometry (GC−MS) analysis of metabolites as indicated. (L) Glycolytic proton efflux rate (glycoPER) was measured in HCT116 (*TP53*$^{-/-}$) cells. Basal and compensatory glycoPER were quantified and shown as histograms ($n = 6$). Data are presented as mean ± SD; $^{*}P < 0.05$, $^{**}P < 0.01$, $^{***}P < 0.001$, $^{****}P < 0.0001$.

(28.8%) showed *TP53* missense mutation, 10 cases (12.5%) featured *TP53* truncation mutation, and 1 case (1.2%) displayed cytoplasmic staining (Fig. S2D). UCHL3 protein levels were significantly higher in *TP53* mutant CRC tissues compared to *TP53* wild-type CRC tissues (Fig. 1I, Fig. S2E). Furthermore, UCHL3 protein was found to be highly expressed in CRC tissues compared to normal epithelial tissues (Fig. S2F and S2G). Additionally, UCHL3 protein levels were notably higher in stage IV CRC tissues compared to stages I-III (Fig. S2H). Importantly, a high expression of UCHL3 was inversely correlated with the overall survival of CRC patients (Fig. S2I). Moreover, UCHL3 protein expression in fresh CRC tissues was also higher than in paired normal epithelial tissues (Fig. S2J). Collectively, these findings demonstrate that UCHL3 is upregulated in CRC, particularly in *TP53*-mutant CRC, and is associated with a poor prognosis for CRC patients. UCHL3 may be involved in the enhanced glycolysis due to *TP53* mutation in CRC, while USP44 was not.

We then investigated the effect of UCHL3 on the metabolic pattern of glucose in CRC. The labeled metabolites of $^{13}C_6$-glucose in glycolysis and the tricarboxylic acid cycle were traced in HCT116 cells with wild-type *TP53* and SW480 cells with *TP53* mutation (Fig. 1J). A notably elevated glycolytic activity was observed in HCT116 cells after the overexpression of UCHL3, as evidenced by the enhanced production of metabolites, including glyceraldehyde-3-phosphate (GAP), 3-phosphoglycerate (3-PG), pyruvate, and lactate. In contrast, levels of the above metabolites were remarkably decreased in SW480 cells after knockdown of UCHL3 (Fig. 1K). These results suggest that UCHL3 significantly promotes glycolysis in CRC. Moreover, we found that UCHL3 slightly facilitated the production of certain metabolites in the tricarboxylic acid cycle, such as succinate, fumarate, and malate (Supporting Information Fig. S3A). This indicates that UCHL3 may also promote oxidative phosphorylation in CRC but to a much lesser extent than glycolysis. In addition, the glycolytic rate assays were performed using the Seahorse XF analyzer. Knockdown of UCHL3 in HCT116 cells with wild-type *TP53* and SW480 cells with *TP53* mutation resulted in a significant reduction in glycolytic proton efflux rate (glycoPER) (Fig. S3B−S3D). Furthermore, overexpression of wild-type or mutant p53 leads to a decrease or acceleration in the glycolytic rate of HCT116 ($TP53^{-/-}$) cells, respectively. However, these effects could be partially reversed by UCHL3 overexpression or knockdown (Fig. 1L, Fig. S3E and S3F). In summary, our findings indicate that UCHL3 is involved in high-level glycolysis caused by *TP53* mutation in CRC.

3.2. UCHL3 is involved in enhanced stem-like properties and 5-FU chemoresistance due to TP53 mutation in CRC

In the TCGA database, we performed KEGG pathway enrichment analysis based on differentially expressed genes in *TP53* mutant and wild-type CRC. The Wnt, Hippo, and PI3K−Akt signaling pathways were activated in *TP53*-mutant CRC, all of which are critical regulators of CSCs (Supporting Information Fig. S4A). Moreover, *TP53*-mutant CRC displayed higher IC_{50} scores of 5-FU and cisplatin compared to *TP53* wild-type CRC (Fig. S4B). These findings further validate that *TP53* mutations contribute to stem-like properties and chemoresistance in CRC.

Furthermore, in TCGA database, we observed that CRC tissues with high expression of *UCHL3* exhibited a higher cancer stem cell-related score (CSC score) (Fig. 2A). Next, we conducted a spheroid formation assay using *TP53*-mutated SW480 cells to enrich tumor stem cells (Fig. 2B). Interestingly, UCHL3 expression in the spheroids was higher than in parental cells (Fig. 2C). These findings suggest that UCHL3 may promote stem-like properties in CRC. Building upon previous results indicating that *TP53* mutation significantly upregulates UCHL3 expression in CRC, we investigated whether UCHL3 is involved in enhanced stem-like properties due to *TP53* mutation. Firstly, we found UCHL3 was highly expressed in CRC cells, particularly in *TP53*-mutant CRC cells, compared to normal epithelial cells (Fig. S4C). Subsequently, UCHL3 was stably overexpressed in HCT116 and RKO cells with wild-type *TP53* and stably knocked down in SW480 and HT29 cells with *TP53* mutation (Fig. 2D, Fig. S4D). Spheroid-formation assays revealed that HCT116 and RKO cells displayed an enhanced self-renewal capacity after stable UCHL3 overexpression, while SW480 and HT29 cells exhibited diminished self-renewal ability after stable UCHL3 knockdown (Fig. 2E, Fig. S4E). We also examined the expression of stem cell markers CD133, CD44, Oct4, Nanog, and Sox2 using flow cytometry and Western blotting. These markers were upregulated in HCT116 and RKO cells upon stably UCHL3 overexpression, while they were downregulated in SW480 and HT29 cells following stably UCHL3 knockdown (Fig. 2F and G, Fig. S4F and S4G). Moreover, knockdown of UCHL3 significantly attenuated the tumorigenicity of tumor stem cells with *TP53* mutation and decreased the expression of the aforementioned stem cell markers in subcutaneous tumors (Fig. 2H, Fig. S4H and S4I). Consequently, UCHL3 is involved in enhanced stem-like properties due to *TP53* mutation in CRC.

Since CSCs play a pivotal role in chemoresistance, we proceeded to investigate whether UCHL3 is involved in chemoresistance due to *TP53* mutation in CRC. Initially, 5-FU-resistant SW480 cells were established (Supporting Information Fig. S5A). Intriguingly, UCHL3 expression was notably higher in 5-FU resistant cells compared to the parental cells (Fig. 2I). In the TCGA database, CRC tissues with high expression of *UCHL3* also exhibited higher IC_{50} scores for 5-FU (Fig. 2J). Furthermore, *UCHL3* mRNA expression displayed a positive correlation with the DNA repair pathway (Fig. S5B). These findings suggest that UCHL3 promotes 5-FU chemoresistance in CRC. Additionally, upon treatment with 5-FU, both wild-type p53 protein in HCT116 cells and mutant p53 protein in SW480 cells were activated. However, UCHL3 expression appeared to decrease in HCT116 cells while significantly increasing in SW480 cells (Fig. 2K). Additionally, the IC_{50} value of 5-FU significantly increased following stable overexpression of UCHL3 in HCT116 and RKO cells, whereas it significantly decreased upon stable knockdown of UCHL3 in SW480 and HT29 cells (Fig. 2L, Fig. S5C). Moreover, when treated with 5-FU, stable overexpression of UCHL3 attenuated apoptosis in HCT116 and RKO cells, while stable knockdown of UCHL3 promoted apoptosis in SW480 and HT29 cells (Fig. 2M, Fig. S5D). To summarize, UCHL3 is involved in 5-FU chemoresistance due to *TP53* mutation in CRC.

In addition, we investigated the effect of UCHL3 on malignant phenotypes of CRC cells. HCT116 and RKO cells were transfected with Flag-UCHL3 plasmid, and SW480 and HT29 cells were transfected with UCHL3-specific siRNA, which were confirmed by Western blotting (Supporting Information Fig. S6A). Overexpression of UCHL3 strengthened the proliferation, migration, invasion, and clonal formation of HCT116 and RKO cells, while knockdown of UCHL3 inhibited these malignant phenotypes of SW480 and HT29 cells (Fig. S6B−S6D). Moreover,

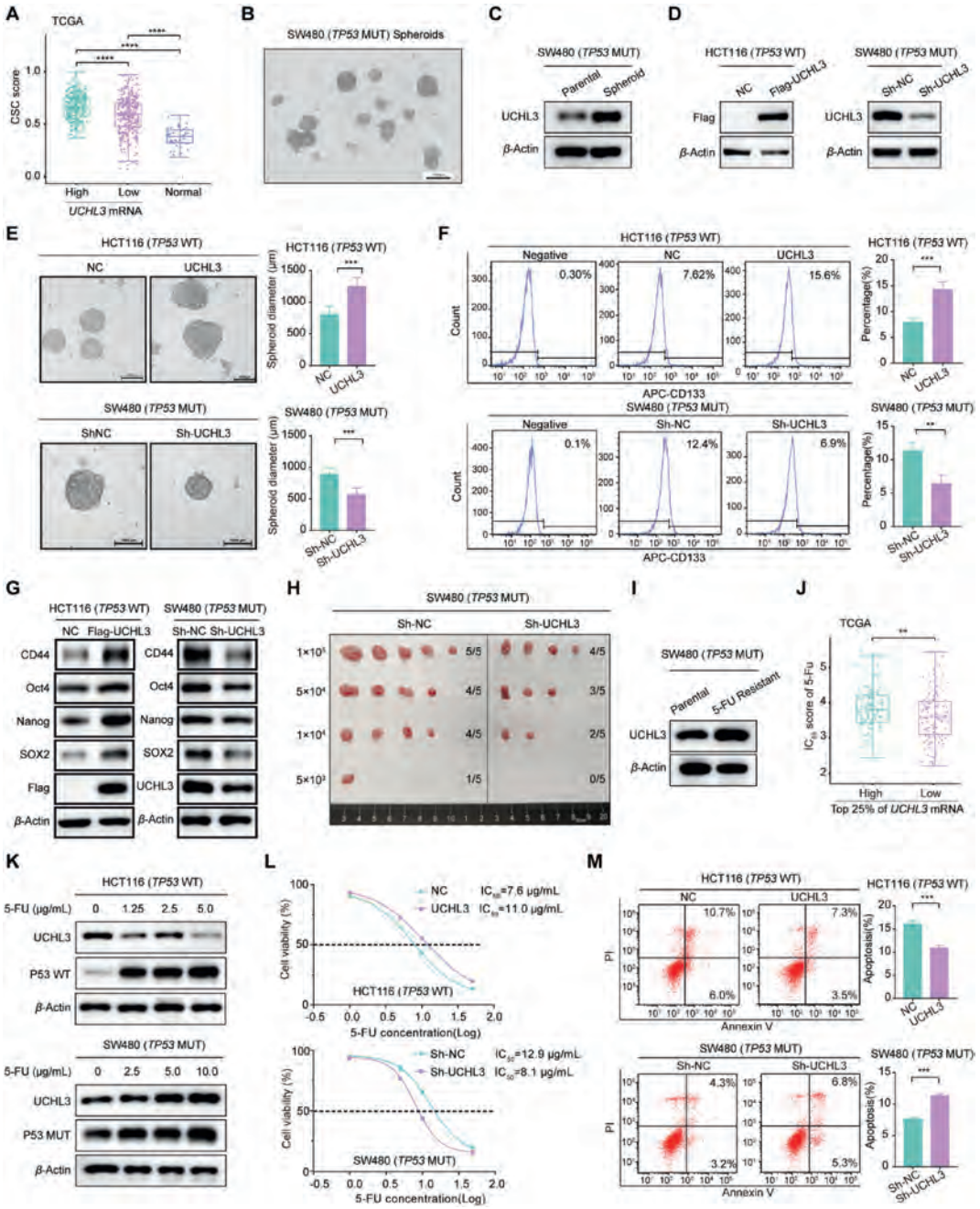

Figure 2 UCHL3 is involved in enhanced stem-like properties and 5-FU chemoresistance due to *TP53* mutation in CRC. (A) Cancer stem-like cell related scores (CSC scores) of CRC tissues with high and low *UCHL3* expression, along with normal colorectal tissues in the TCGA database. (B) Representative image of SW480 (*TP53* MUT) spheroids. Scale bar, 1000 μm. (C) Immunoblotting of UCHL3 in SW480 (*TP53* MUT) parental cells and spheroids. (D) Immunoblotting of UCHL3 in HCT116 (*TP53* WT) cells after stable UCHL3 overexpression and SW480 (*TP53* MUT) cells after stable UCHL3 knockdown. (E) Self-renewal abilities of HCT116 (*TP53* WT) and SW480 (*TP53* MUT) cells were assessed by spheroids formation assays ($n = 5$). Scale bar, 1000 μm. (F) Percentage of HCT116 (*TP53* WT) and SW480 (*TP53* MUT) cells with positive CD133 expression analyzed by flow cytometry ($n = 3$). (G) Immunoblotting of stem cell markers in HCT116 (*TP53* WT) and SW480 (*TP53* MUT) cells. (H) *In vivo* stem cell tumorigenesis assay after UCHL3 knockdown in SW480 (*TP53* MUT) cells ($n = 5$ mice per group). (I) Immunoblotting of UCHL3 in SW480 (*TP53* MUT) parental cells and 5-FU resistant cells. (J) Half maximal inhibitory concentration (IC_{50}) scores of 5-FU in CRC tissues with high and low *UCHL3* expression in TCGA database. (K) Immunoblotting of UCHL3 and P53 in HCT116 (*TP53* WT) and SW480 (*TP53* MUT) cells treated with incremental concentrations of 5-FU for 36 h. (L) IC_{50} values of HCT116 (*TP53* WT) and SW480 (*TP53* MUT) cells measured by cell counting kit-8 (CCK8) assay after treatment with different concentrations of 5-FU (1−50 μg/mL) for 48 h. (M) Flow cytometry analysis of apoptosis after treatment with 5-FU (10 μg/mL) in HCT116 (*TP53* WT) and SW480 (*TP53* MUT) cells for 48 h ($n = 3$). Data are presented as mean ± SD; $^{**}P < 0.01$, $^{***}P < 0.001$, $^{****}P < 0.0001$.

in vivo xenograft assay demonstrated that the proliferation rate of subcutaneous tumors was significantly reduced after knocking down UCHL3 in SW480 cells, which was further supported by the decreased Ki-67 expression in subcutaneous tumors (Supporting Information Fig. S7).

3.3. UCHL3 interacts with ENO1 and stabilizes the ENO1 protein through deubiquitination

Considering the important role of UCHL3 in inducing LDHA expression as determined by a DUBs plasmid library screening at the beginning of our study, LDHA was initially selected to explore the downstream molecular mechanism of UCHL3. However, the interaction between UCHL3 and LDHA proteins in HCT116 cells with wild-type *TP53* and SW480 cells with *TP53* mutation was not confirmed through Co-IP assays (Supporting Information Fig. S8A). Moreover, UCHL3 was found to positively regulate both mRNA and protein expression levels of LDHA (Fig. S8B). These results suggest that UCHL3 may affect LDHA protein expression by influencing the mRNA level of *LDHA*, rather than through protein−protein interactions and exerting deubiquitinating enzyme activity to influence the ubiquitination modification of LDHA proteins. We discontinued further research on the indirect regulatory mechanisms through which UCHL3 promotes LDHA expression. Immunoprecipitation (IP) was performed to identify proteins that interact with UCHL3, and band 3 in silver-stained polyacrylamide gel was subjected to mass spectrometry (MS) analysis (Fig. 3A). Among the candidate proteins listed in Supporting Information Table S4, ENO1 was chosen for further analysis not only due to its role as a key enzyme in glycolysis but also because it has been reported to promote stem-like properties and chemotherapy resistance in a variety of tumors. Moreover, in the TCGA database, CRC tissues with high *ENO1* expression tended to have a higher CSC score (Fig. S8C). *ENO1* mRNA levels were also positively associated with the DNA repair pathway (Fig. S8D). Additionally, we confirmed that ENO1 expression was higher in spheroids and 5-FU-resistant cells than in parental CRC cells (Fig. S8E).

Subsequently, the interaction between UCHL3 and ENO1 proteins in HCT116 cells with wild-type *TP53* and SW480 cells with *TP53* mutation was confirmed through Co-IP assays (Fig. 3B). UCHL3 overexpression increased ENO1 protein expression in HCT116 cells, whereas UCHL3 knockdown decreased ENO1 protein expression in SW480 cells. Notably, no significant alterations were observed in *ENO1* mRNA expression (Fig. 3C). As UCHL3 is a member of deubiquitinating enzymes, it is likely that UCHL3 decreases the ubiquitination of ENO1, thereby delaying its ubiquitin-proteasome degradation, independent of ENO1 transcription. Indeed, treatment with the proteasome inhibitor MG132 in HCT116 and SW480 cells rendered UCHL3 incapable of regulating ENO1 protein levels (Fig. 3D). Furthermore, UCHL3 overexpression decelerated the degradation of ENO1 protein in HCT116 cells, while UCHL3 knockdown accelerated the degradation of ENO1 protein in SW480 cells (Fig. 3E). In addition, UCHL3 overexpression reduced the ubiquitination of endogenous ENO1 protein in HCT116 cells, whereas UCHL3 knockdown increased the ubiquitination of endogenous ENO1 protein in SW480 cells (Fig. 3F). As different types of polyubiquitin linkages mediate distinct biological functions, we expressed Flag-tagged ENO1 in 293T cells together with various ubiquitin mutants (K6, K11, K27, K29, K33, K48, K63), all of which contained just one indicated lysine available for polylinkage. Notably, overexpressing UCHL3 mainly decreased K27- and K48-linked ubiquitination of ENO1 (Fig. 3G, Fig. S8F). We compared the protein sequence of ENO1 in various species and identified five conserved lysine residues (K126, K193, K202, K256, K420) in ENO1 protein (Fig. S8G). We generated ENO1 mutants by substituting lysine for arginine. The K256R and K420R substitution rather than other point mutations abolished UCHL3-mediated deubiquitination of ENO1 (Fig. 3H, Fig. S8H). These results suggest that UCHL3 interacts with ENO1 and stabilizes the ENO1 protein through deubiquitination, and that K256 and K420 are critical sites for ubiquitination and the stability of ENO1.

3.4. UCHL3 promotes glycolysis, stem-like properties, and 5-FU chemoresistance through regulating ENO1

We then investigated whether ENO1 is involved in the role of UCHL3 in promoting glycolysis, stem-like properties, and 5-FU chemoresistance in CRC. Firstly, immunohistochemical analysis of UCHL3 and ENO1 proteins was performed on specimens from 41 patients with CRC (Fig. 4A). Kendall's Tau-b test demonstrated a statistically significant positive correlation between UCHL3 and ENO1 protein levels (Fig. 4B). Additionally, liner correlation analysis indicated a positive association between the staining scores of UCHL3 and ENO1 (Fig. 4C). Furthermore, knockdown of UCHL3 resulted in decreased expression of ENO1 protein in subcutaneous tumors of mice (Fig. S7C).

Next, we conducted rescue experiments using RKO cells with wild-type *TP53* and SW480 cells with *TP53* mutation. ENO1 was overexpressed in RKO and SW480 cells with stable knockdown of UCHL3 (Supporting Information Fig. S9A). Stable knockdown of UCHL3 resulted in a significant reduction in glycolytic rate in RKO and SW480 cells, which were partially reversed by ENO1 overexpression (Fig. 4D and Fig. S9B−S9D). Additionally, stable knockdown of UCHL3 reduced self-renewal ability and the expression of stem cell markers CD133, CD44, Oct4, Nanog, and Sox2 in RKO and SW480 cells, which were partly restored by ENO1 overexpression (Fig. 4E−G and Fig. S9E−S9G). Furthermore, the IC_{50} values of 5-FU were significantly decreased upon stable knockdown of UCHL3 in RKO and SW480 cells, but they were elevated again after ENO1 overexpression (Fig. 4H and Fig. S9H). Upon treatment with 5-FU, ENO1 upregulation also partially counteracted the high level of apoptosis induced by stable knockdown of UCHL3 in RKO and SW480 cells (Fig. 4I and Fig. S9I). Overall, our findings suggest that UCHL3 promotes glycolysis, stem-like properties, and 5-FU chemoresistance through regulating ENO1.

In addition, stable knockdown of UCHL3 suppressed the proliferation, migration, invasion, and clone formation of RKO and SW480 cells, which were partially restored by ENO1 overexpression (Supporting Information Fig. S10). These findings suggest that UCHL3 promotes the malignant phenotype of CRC through regulating ENO1.

3.5. TP53 mutations activate the JAK2−STAT3 pathway to promote UCHL3 expression, which can be effectively blocked by pacritinib

We screened a library of FDA-approved compounds to identify drugs that significantly suppress UCHL3 expression in *TP53* mutant CRC cells. Our expectation is to elucidate the mechanism by which *TP53* mutations upregulate UCHL3 expression in CRC

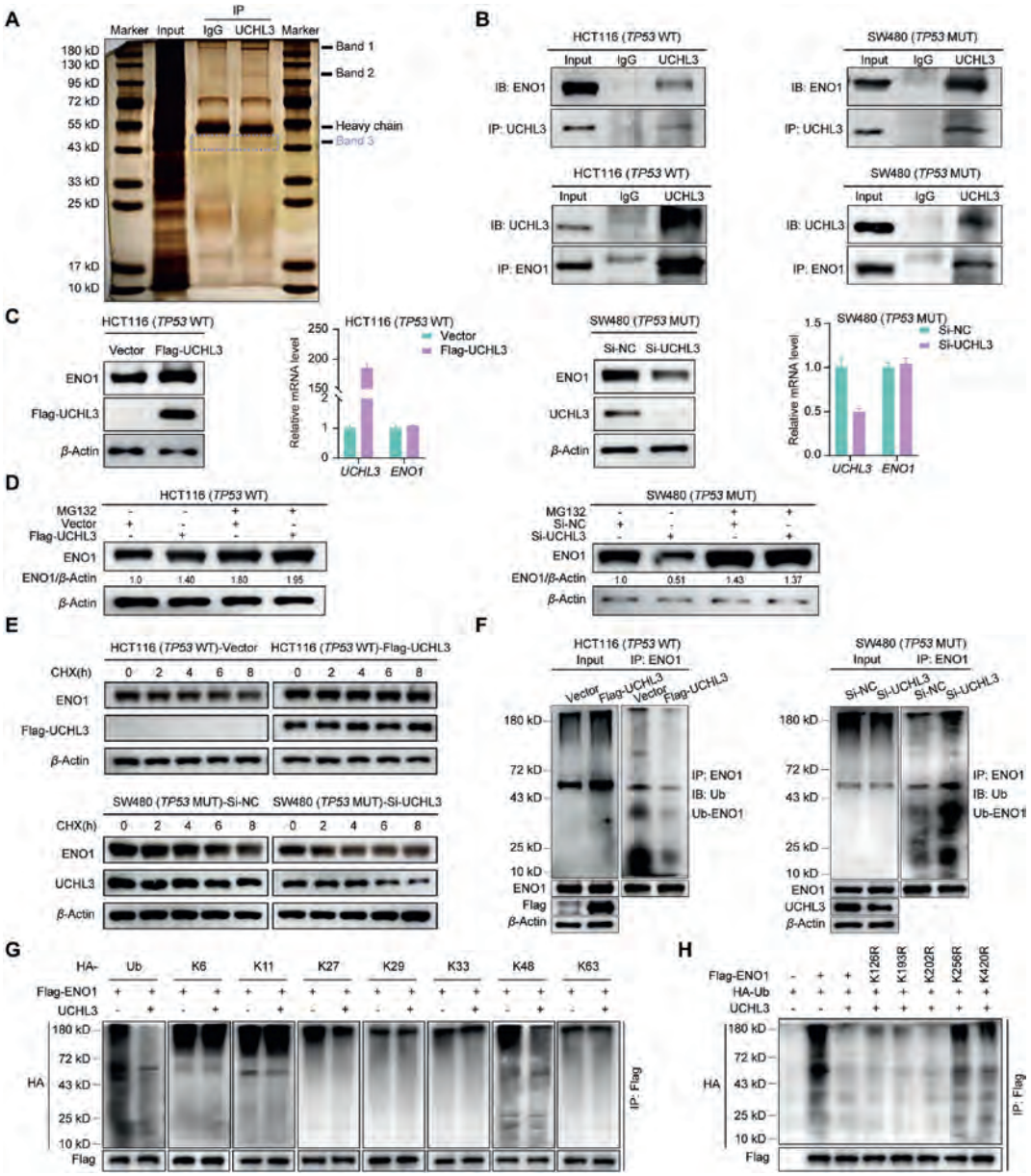

Figure 3 UCHL3 interacts with ENO1 and stabilizes the ENO1 protein through deubiquitination. (A) Lysates of SW480 (*TP53* MUT) cells were subjected to immunoprecipitation (IP) using anti-IgG or anti-UCHL3 antibodies. Band 3 in Silver-stained polyacrylamide gel was identified by mass spectrometry (MS). (B) The interaction between UCHL3 and ENO1 in HCT116 (*TP53* WT) and SW480 (*TP53* MUT) cells was confirmed by Coimmunoprecipitation (Co-IP) assays. (C) Immunoblotting and RT-qPCR analysis of UCHL3 and ENO1 expression levels in HCT116 (*TP53* WT) and SW480 (*TP53* MUT) cells ($n = 3$). (D) Immunoblotting of ENO1 and UCHL3 in HCT116 (*TP53* WT) and SW480 (*TP53* MUT) cells after UCHL3 overexpression or knockdown for 36 h, followed by MG132 (10 μmol/L) treatment for 12 h. (E) UCHL3 delayed ENO1 protein degradation. HCT116 (*TP53* WT) and SW480 (*TP53* MUT) cells after UCHL3 overexpression or knockdown for 48 h were incubated with cycloheximide (CHX, 100 μg/mL) for indicated time points, and ENO1 protein expression was analyzed by WB. (F) UCHL3 decreased ubiquitination modifications of ENO1 protein. After transfection with UCHL3 plasmids or siRNA for 48 h, HCT116 (*TP53* WT) and SW480 (*TP53* MUT) cell lysates were immunoprecipitated with anti-ENO1 antibody, followed by Western blotting of the precipitated proteins with anti-Ub antibody. (G) Immunoblot analysis of lysates from 293T cells transfected with HA-tagged ubiquitin (HA-Ub), HA-tagged K6-linked ubiquitin (HA-K6-Ub), HA-tagged K11-linked ubiquitin (HA-K11-Ub), HA-tagged K27-linked ubiquitin (HA-K27-Ub), HA-tagged K29-linked ubiquitin (HA-K29-Ub), HA-tagged K33-linked ubiquitin (HA-K33-Ub), HA-tagged K48-linked ubiquitin (HA-K48-Ub), or HA-tagged K63-linked ubiquitin (HA-K63-Ub) and Flag-ENO1, with or without UCHL3, followed by IP with anti-Flag M2 beads, then probed with anti-HA. (H) Immunoblot analysis of lysates from 293T cells transfected with HA-tagged ubiquitin, UCHL3, Flag-ENO1, or indicated mutant Flag-ENO1, followed by IP with anti-Flag M2 beads, then probed with anti-HA. Data are presented as mean ± SD.

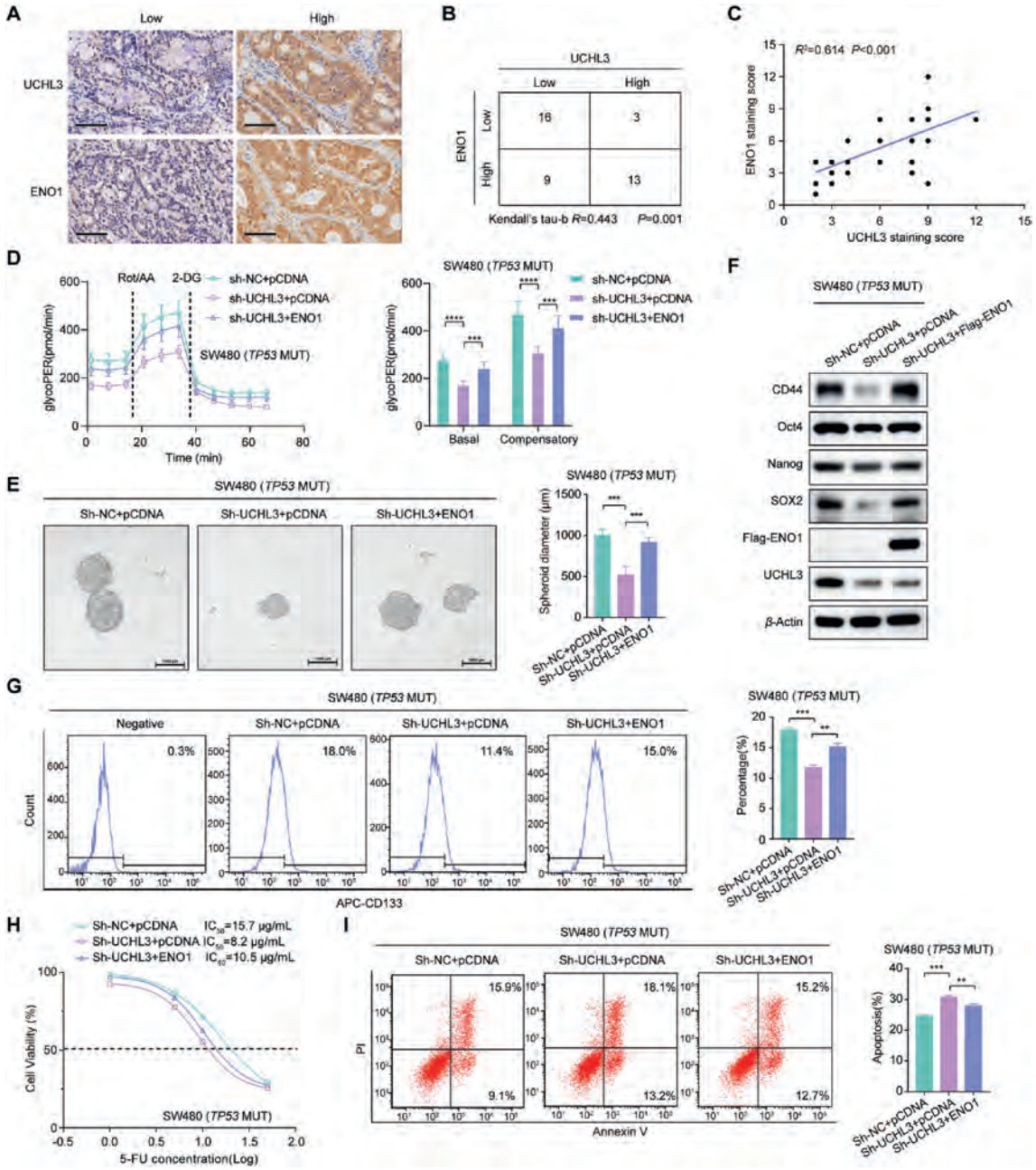

Figure 4 UCHL3 promotes glycolysis, stem-like properties, and 5-FU chemoresistance through regulating ENO1. (A) IHC analysis of UCHL3 and ENO1 was performed on specimens from 41 CRC patients. Scale bar, 100 μm. (B) The correlation between UCHL3 and ENO1 protein levels was assessed using Kendall's tau-b test. (C) The staining scores between UCHL3 and ENO1 protein were assessed through linear correlation analysis. (D) GlycoPER was measured in SW480 (*TP53* MUT) cells. Basal and compensatory glycoPER were quantified and presented as histograms ($n = 6$). (E) Analysis of the self-renewal abilities of SW480 (*TP53* MUT) cells by spheroids formation assays ($n = 5$). Scale bar, 1000 μm. (F) Immunoblotting of stem cell markers in SW480 (*TP53* MUT) cells. (G) Analysis of the percentage of SW480 (*TP53* MUT) cells with positive CD133 expression by flow cytometry ($n = 3$). (H) IC_{50} values of SW480 (*TP53* MUT) cells were measured by CCK8 assay after treatment with different concentrations of 5-FU (1−50 μg/mL) for 48 h. (I) Flow cytometry analysis of apoptosis after treatment with 5-FU (10 μg/mL) in SW480 (*TP53* MUT) cells for 48 h ($n = 3$). Data are presented as mean ± SD; $^{**}P < 0.01$, $^{***}P < 0.001$, $^{****}P < 0.0001$.

and to repurpose existing drugs for the treatment of *TP53*-mutant CRC (Fig. 5A). Among the compounds listed in Supporting Information Table S5, particularly noteworthy were Filgotinib and Pacritinib, both small molecule JAK inhibitors (Fig. 5B). Filgotinib targeted JAK1, JAK2 and JAK3, while pacritinib specifically inhibited JAK2. Considering that the JAK2−STAT3 pathway is a critical regulator of CSCs (Fig. 5C), we speculated that inhibiting the JAK2−STAT3 pathway in *TP53* mutant CRC cells could effectively suppress UCHL3 expression. Therefore, Pacritinib was chosen for further investigation.

The IC_{50} value of pacritinib was initially determined in SW480 and HT29 cells with *TP53* mutation (Supporting Information

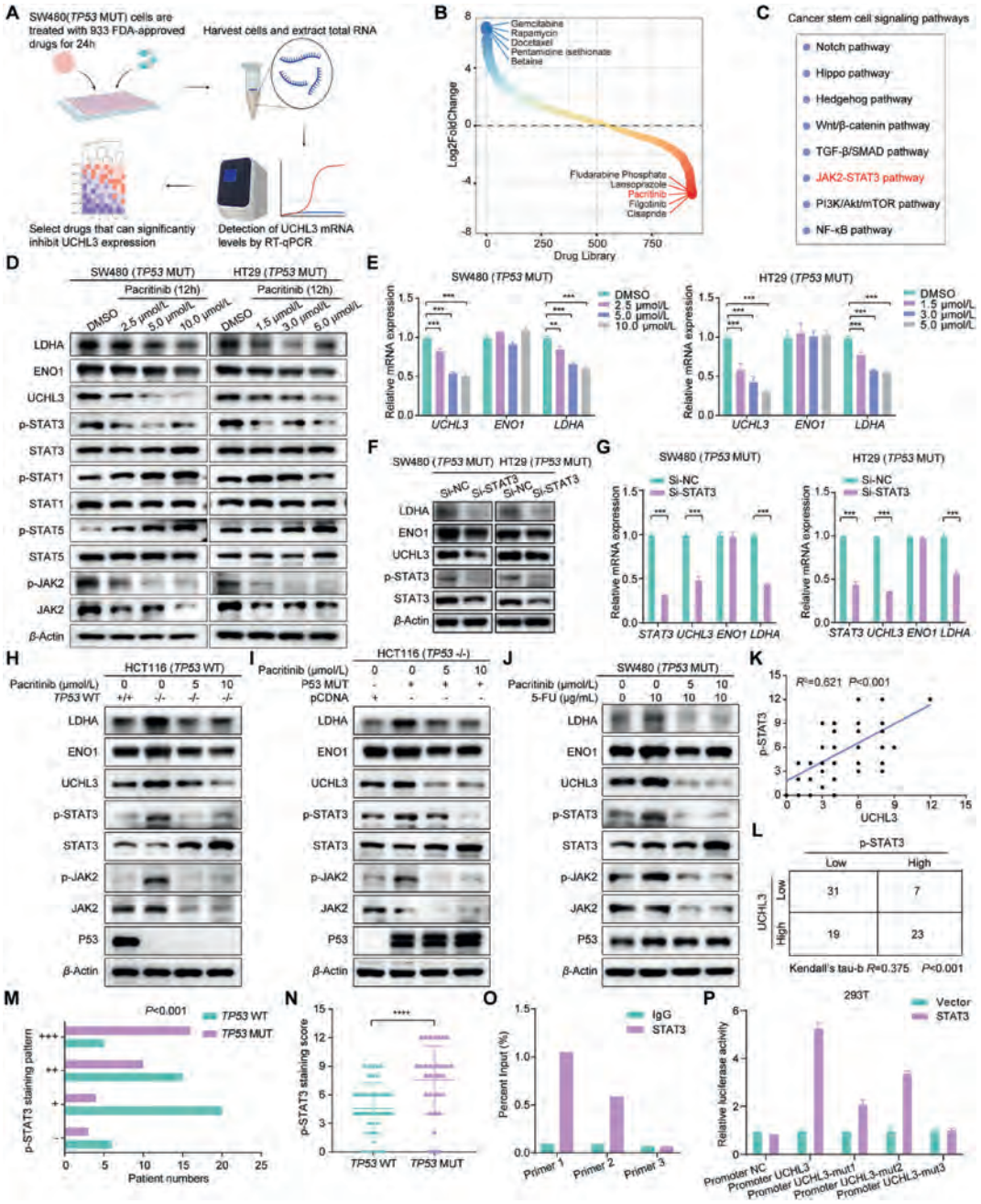

Figure 5 *TP53* mutations activate the JAK2−STAT3 pathway to promote UCHL3 expression, which can be effectively blocked by pacritinib. (A) An outline of the drug screening procedure. (B) Sequencing chart of *UCHL3* differential expression after treatment with specific drugs. (C) Cancer stem cell related signaling pathways were listed. (D) Immunoblotting of indicated proteins in SW480 (*TP53* MUT) and HT29 (*TP53* MUT) cells treated with different concentrations of pacritinib for 12 h. (E) RT-qPCR analysis of *UCHL3*, *ENO1*, and *LDHA* in SW480 (*TP53* MUT) and HT29 (*TP53* MUT) cells treated with different concentrations of pacritinib for 12 h ($n = 3$). (F) Immunoblotting of indicated proteins in SW480 (*TP53* MUT) and HT29 (*TP53* MUT) cells transfected with STAT3 siRNA for 48 h. (G) RT-qPCR analysis of *STAT3*, *UCHL3*, *ENO1* and *LDHA* in SW480 (*TP53* MUT) and HT29 (*TP53* MUT) cells transfected with STAT3 siRNA for 36 h ($n = 3$). (H) Immunoblotting of indicated proteins in HCT116 (*TP53* WT) cells with wild-type P53 knocked out followed by treatment with different concentrations of pacritinib for 12 h. (I) Immunoblotting of indicated proteins in HCT116 ($TP53^{-/-}$) cells after overexpression of P53 MUT for 36 h and treated with different concentrations of pacritinib for 12 h. (J) Immunoblotting of indicated proteins in SW480 (*TP53* MUT) cells treated with different concentrations of 5-FU for 48 h, followed by different concentrations of pacritinib for 12 h. (K) Assessment of the correlation of p-STAT3 and UCHL3 staining scores by linear correlation analysis. (L) Assessment of the correlation of p-STAT3 and UCHL3 protein levels using Kendall's tau-b test. (M) Comparison of the distribution of various p-STAT3 staining patterns in CRC tissues with wild-type and mutant *TP53*. (N) Comparison of p-STAT3 staining scores in CRC tissues with wild-type and mutant *TP53*. (O) Chromatin immunoprecipitation (ChIP) assay was performed with STAT3 antibody and mouse immunoglobulin (IgG), followed by detection of UCHL3 promoter by RT-qPCR. (P) Detection and analysis of luciferase activity in HEK293T co-transfected with STAT3 and UCHL3 promoter/mutant1/mutant2/mutant3/pGL-3 basic vector plasmid. Data are presented as mean ± SD; $^{**}P < 0.01$, $^{***}P < 0.001$, $^{****}P < 0.0001$.

Fig. S11A). As expected, the protein levels of JAK2, phosphorylated JAK2, phosphorylated STAT3, UCHL3, ENO1 and LDHA progressively decreased with increasing concentration of Pacritinib (Fig. 5D). Furthermore, *UCHL3* and *LDHA* mRNA expression was gradually suppressed, while *ENO1* mRNA expression remained unchanged (Fig. 5E). These findings suggest that Pacritinib may enhance the ubiquitination of ENO1 protein by inhibiting UCHL3 expression without affecting the transcription of ENO1. Additionally, UCHL3, ENO1, LDHA, and phosphorylated STAT3 in SW480 and HT29 cells were progressively suppressed over time after treatment with a specific concentration (0.5-fold IC_{50}) of Pacritinib (Fig. S11B). Similarly, *UCHL3* and *LDHA* mRNA expression was gradually suppressed, while *ENO1* mRNA remained unaltered (Fig. S11C). Furthermore, knockdown of STAT3 in SW480 and HT29 cells resulted in a significant reduction in UCHL3, ENO1, and LDHA protein levels, along with a marked decrease in *UCHL3* and *LDHA* mRNA expression, while *ENO1* mRNA expression remained unaffected (Fig. 5F and G). These data collectively indicate that Pacritinib can inhibit UCHL3, ENO1, and LDHA expression in SW480 and HT29 cells with *TP53* mutation by blocking the JAK2−STAT3 pathway.

Next, we investigated whether it was the activation of JAK2−STAT3 pathway that resulted in elevated UCHL3 expression in *TP53*-mutant CRC. Both deletion of wild-type *TP53* in HCT116 cells and overexpression of mutant p53 protein in HCT116 ($TP53^{-/-}$) cells significantly activated the JAK2−STAT3 pathway and induced UCHL3, ENO1 and LDHA expression, which was effectively counteracted by Pacritinib treatment (Fig. 5H and I). In contrast, both overexpression of wild-type p53 protein in HCT116 ($TP53^{-/-}$) cells and knockdown of mutant p53 protein in SW480 cells suppressed the JAK2−STAT3 pathway, UCHL3, ENO1, and LDHA expression (Fig. S11D and S11E). Furthermore, when treated with 5-FU alone, both mutant p53 protein and the JAK2−STAT3 pathway were significantly activated in SW480 cells, leading to increased UCHL3, ENO1, and LDHA expression. However, this process could be effectively blocked by co-treatment with pacritinib (Fig. 5J). Moreover, immunohistochemical analysis of phosphorylated STAT3 was performed on the same tissue array as before (Fig. S11F). Liner correlation analysis revealed a significantly positive correlation between the staining score of phosphorylated STAT3 and UCHL3 protein (Fig. 5K). Kendall's Tau-b test also indicated a positive correlation between phosphorylated STAT3 and UCHL3 protein levels in CRC tissues (Fig. 5L). The phosphorylated STAT3 level was significantly higher in CRC tissues with mutant *TP53* compared to those with wild-type *TP53* (Fig. 5M and N). Furthermore, two potential STAT3 binding sites (−632 to −622 bp, −457 to −448 bp) were identified in the UCHL3 promoter region within the NCBI combined JASPAR database (Fig. S11G). Subsequently, a ChIP assay was conducted, demonstrating that the STAT3 antibody specifically enriched the predicted UCHL3 promoter fragments (Fig. 5O). Additionally, the luciferase reporter assay confirmed a significant activation of the UCHL3 promoter by STAT3 overexpression. However, when both binding sites were simultaneously deleted, STAT3 overexpression failed to activate the UCHL3 promoter (Fig. 5P). These results strongly support that STAT3 binds primarily to the two predicted sites in the UCHL3 promoter region, thereby activating UCHL3 transcription and expression. In summary, these findings collectively suggest that the elevated expression of UCHL3 in *TP53*-mutant CRC is, at least partially, attributed to the activation of the JAK2−STAT3 pathway, a process effectively reversible by Pacritinib treatment.

3.6. Pacritinib suppresses glycolysis and enhances 5-FU chemotherapy sensitivity in TP53-mutant CRC

We next investigated whether Pacritinib could inhibit glycolysis and improve the sensitivity of 5-FU chemotherapy in CRC with *TP53* missense and truncation mutations. Since there are no CRC cell lines with *TP53* truncation mutations, and as truncation mutations typically yield truncated proteins that are usually degraded shortly after translation, HCT116 ($TP53^{-/-}$) cells with a complete knockout of the wild-type *TP53* gene were used to mimic *TP53* truncation mutant cells. Initially, glycolytic rate assays were performed, and it was noted that overexpression of p53 missense mutant significantly increased the glycolytic rate in HCT116 ($TP53^{-/-}$) cells, which was markedly diminished with pacritinib treatment (Fig. 6A, Supporting Information Fig. S12A). Similarly, the glycolytic rate of SW480 cells with *TP53* missense mutation significantly decreased following pacritinib treatment (Fig. 6B, Fig. S12B). Furthermore, compared to HCT116 cells with wild-type *TP53*, the glycolytic rate was significantly elevated in HCT116 ($TP53^{-/-}$) cells with complete *TP53* knockout, which could be effectively suppressed upon treatment with pacritinib (Fig. S12C and S12D). These results indicate that pacritinib can effectively reverse the high-level glycolysis in CRC cells with *TP53* truncation and missense mutations.

In addition, compared to HCT116 cells with wild-type *TP53*, pacritinib more effectively suppressed the self-renewal ability of HCT116 ($TP53^{-/-}$) cells with complete *TP53* knockout and SW480 cells with *TP53* missense mutation (Fig. 6C, Fig. S12E). Furthermore, we investigated the combined effect of pacritinib and 5-FU treatment *in vitro*. Compared to HCT116 cells with wild-type *TP53*, treatment with 5-FU alone resulted in lower levels of apoptosis and a higher number of surviving clones in HCT116 ($TP53^{-/-}$) cells with complete *TP53* knockout and SW480 cells with *TP53* missense mutation. In contrast, the combined treatment significantly induced apoptosis and decreased the number of surviving clones (Fig. 6D and E, Fig. S12F, Supporting Information Fig. S13A). These results suggest that pacritinib can effectively inhibit stem-like properties and enhance the sensitivity of 5-FU chemotherapy in CRC cells with *TP53* truncation and missense mutations *in vitro*.

Moreover, a subcutaneous xenograft tumor model was established in nude mice using SW480 cells with *TP53* missense mutation (Fig. 6F). When administered individually, 5-FU or pacritinib moderately attenuated tumor growth, but their combined treatment significantly suppressed tumor growth (Fig. 6G−I). Notably, the combination treatment was well-tolerated, with only a minimal body weight loss observed (Fig. 6J). IHC analysis of xenograft tumors revealed a significant reduction in the expression of the proliferation marker Ki-67 and an increase in the apoptotic marker cleaved caspase-3 with the combined treatment, as compared to 5-FU treatment alone (Fig. 6K). Furthermore, individual treatment with 5-FU significantly activated the mutant p53 proteins and p-STAT3−UCHL3−ENO1 axis in tumors, whereas the combination treatment effectively inhibited the activation of p-STAT3−UCHL3−ENO1 axis (Fig. 6K). Moreover, patient-derived xenograft (PDX) tumor models with wild-type *TP53* and *TP53* missense mutations were established (Fig. 7A). In *TP53*-mutant PDX models, the combination treatment significantly suppressed tumor growth, as compared to individual 5-FU treatment (Fig. 7B−E). Conversely, no such effect was observed in PDX models with wild-type *TP53* (Fig. S13B−S13E). The combined treatment was well-tolerated by the mice, with no significant

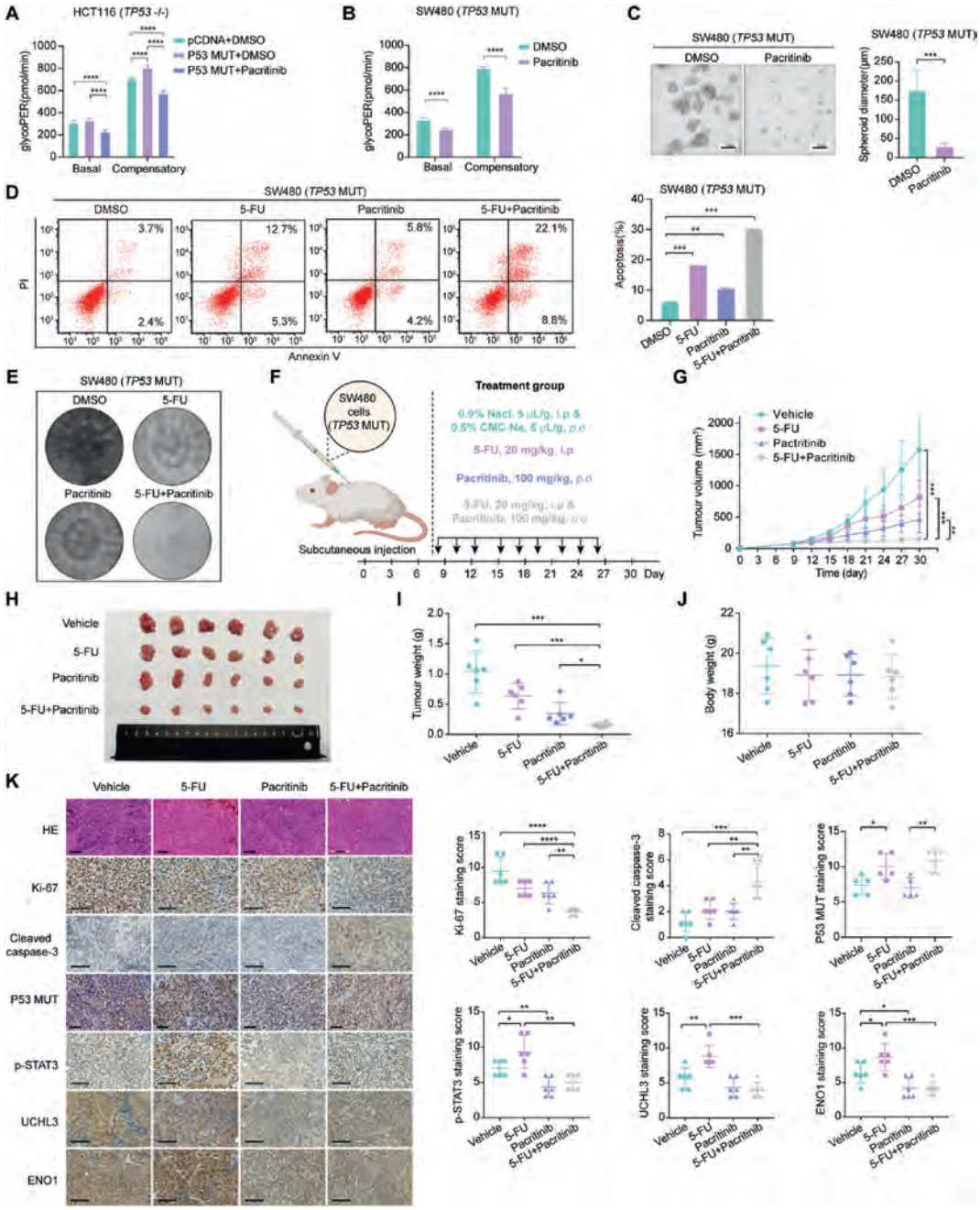

Figure 6 Pacritinib suppresses glycolysis and enhances 5-FU chemotherapy sensitivity in *TP53*-mutant CRC. (A) GlycoPER was measured in HCT116 (*TP53*$^{-/-}$) cells after overexpression of P53 missense mutant for 36 h or simultaneous overexpression of P53 missense mutant for 36 h and treatment with pacritinib (5 μmol/L) for 4 h. Basal and compensatory glycoPER were quantified and shown as histograms ($n = 6$). (B) GlycoPER was measured in SW480 cells with *TP53* missense mutation after treatment with pacritinib (5 μmol/L) for 4 h. Basal and compensatory glycoPER were quantified and shown as histograms ($n = 6$). (C) Tumor sphere formation of SW480 cells with *TP53* missense mutation treated with pacritinib (0.5 μmol/L) for 5 days ($n = 5$). Scale bar, 200 μm. (D) Flow cytometry analysis of apoptosis in SW480 cells with *TP53* missense mutation treated with 5-FU (10 μg/mL) in the presence or absence of pacritinib (0.5 μmol/L) for 48 h ($n = 3$). (E) Therapeutic effect on SW480 cells with *TP53* missense mutation treated with 5-FU (10 μg/mL) with or without pacritinib (0.5 μmol/L) for 48 h *in vitro*. (F) Schematic diagram of combined treatment with 5-FU and pacritinib *in vivo*. (G) Growth curve of xenograft tumors in nude mice in different treatment groups ($n = 6$). (H) The image shows the tumor sizes at the end of the experiment. Scale bar, 1 cm. (I) Scatter graph shows the tumor weight of each group at the end of treatment. (J) The body weight of nude mice after treatment from 4 groups. (K) Left, representative hematoxylin and eosin (H&E) staining and IHC images of subcutaneous tumors from mice with different treatments. Scale bar, 100 μm. Right, comparison of IHC scores for indicated proteins. Data are presented as mean ± SD; $^{*}P < 0.05$, $^{**}P < 0.01$, $^{***}P < 0.001$, $^{****}P < 0.0001$.

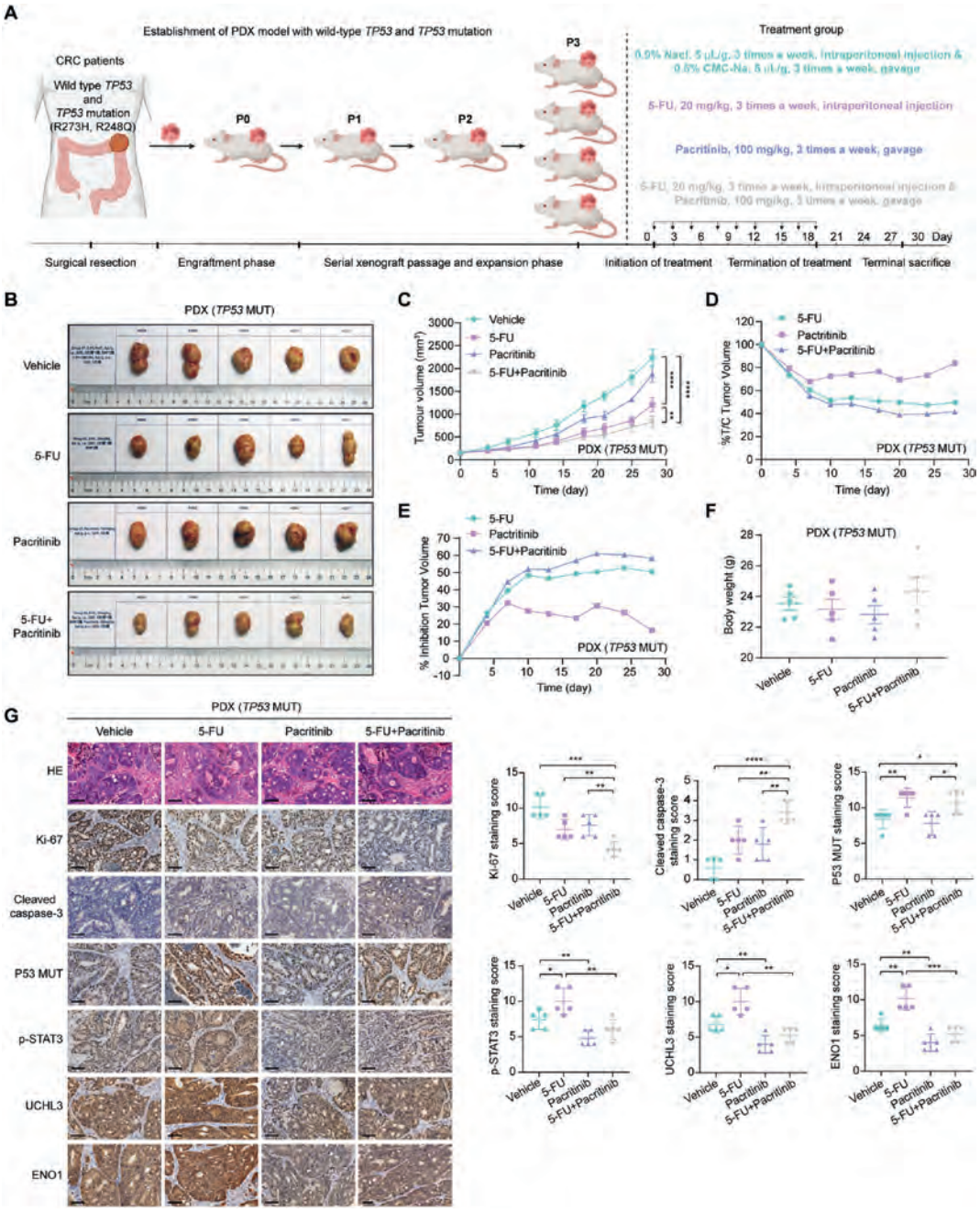

Figure 7 Pacritinib enhances 5-FU chemotherapy sensitivity in patient-derived xenograft (PDX) tumors with *TP53* missense mutation. (A) Left, Construction process of PDX tumors with wild-type *TP53* and *TP53* missense mutation. Right, Treatment of PDX tumors with the vehicle, 5-FU at 20 mg/kg, pacritinib at 100 mg/kg, or both, administered 3 times a week for a total of 9 times. (B) The image shows the sizes of PDX tumors with *TP53* missense mutation at the end of experiment. Scale bar, 1 cm. (C) Growth curve of PDX tumors with *TP53* missense mutation in various treatment groups ($n = 5$). (D, E) Proliferation rate curve (D) and inhibition rate curve (E) of PDX tumors with TP53 missense mutation in each treatment group. %T/C Tumor volume = mean (T)/mean (C) × 100%. % Inhibition tumor volume = (mean (C)−mean (T))/mean (C) × 100%. T represents the current group value, and C represents the control group value. (F) The body weight of NOD/SCID mice after treatment from 4 groups. (G) Left, Representative H&E staining and IHC images of PDX tumors with *TP53* missense mutation from different treatment groups. Scale bar, 100 μm. Right, Comparison of IHC scores for indicated proteins. Data are presented as mean ± SD; $*P < 0.05$, $**P < 0.01$, $***P < 0.001$, $****P < 0.0001$.

loss in body weight (Fig. 7F, Fig. S13F). Additionally, IHC analysis of *TP53*-mutant PDX tumors confirmed that combination treatment resulted in reduced Ki-67 expression and increased cleaved caspase-3 expression compared to treatment with 5-FU alone (Fig. 7G). In *TP53*-mutant PDX tumors treated with 5-FU alone, the activation of p53 proteins and the p-STAT3−UCHL3−ENO1 axis was observed, but the combined treatment significantly suppressed the activation of p-STAT3−UCHL3−ENO1 axis (Fig. 7G). However, in PDX tumors with wild-type *TP53*, no significant differences were observed in

the expression levels of Ki-67 and cleaved caspase-3 between the combination treatment group and the 5-FU treatment group (Fig. S13G). Although p53 proteins were similarly activated in PDX tumors harboring wild-type *TP53* following 5-FU treatment, the activation of p-STAT3−UCHL3−ENO1 axis was not observed (Fig. S13G). In conclusion, these findings further confirm that Pacritinib can enhance sensitivity to 5-FU chemotherapy in CRC with *TP53* missense mutations *in vivo*.

4. Discussion

In the clinical management of CRC, it has become a routine paradigm to evaluate the presence of *TP53* mutation through immunohistochemical detection of p53 on resected tumor specimens. Approximately 60% of CRC patients exhibit *TP53* mutations, which are strongly associated with tumor progression, resistance to chemotherapy, and an unfavorable prognosis[28]. Despite ongoing efforts to develop p53-based therapies for nearly three decades, numerous challenges persist, and no effective drugs have been successfully applied in the clinical treatment of CRC[19]. Therefore, it is imperative to identify novel alternative therapeutic targets to improve the prognosis of CRC patients with *TP53* mutations.

DUBs play a pivotal role in maintaining protein stability by removing ubiquitin from protein substrates, thereby shielding them from degradation[29,30]. Emerging evidence suggests that DUBs are involved in tumor metabolic reprogramming and chemotherapy resistance[31,32]. However, it remains unknown whether any of the DUBs contribute to high-level glycolysis, enhanced stem-like properties, and 5-FU chemoresistance in *TP53*-mutant CRC. In this study, we identified UCHL3, a member of the DUBs family, as a contributor to high-level glycolysis caused by *TP53* mutations in CRC. Isotopic tracing of glucose metabolic flow showed that UCHL3 not only remarkably facilitated the production of metabolites in glycolysis, but also slightly up-regulated the levels of certain metabolites in the TCA cycle, suggesting that UCHL3 comprehensively accelerated glucose metabolic flow in CRC. Since the effect of UCHL3 on oxidative phosphorylation is much weaker than that on glycolysis, our study focused on the glycolysis pathway, while the oxidative phosphorylation pathway needs to be further investigated in the future. Additionally, we identified UCHL3 for the first time as a downstream effector regulated by p53. The inactivation or gain-of-function mutation of p53 resulted in an upregulation of UCHL3 expression in *TP53*-mutant CRC. Previous studies have demonstrated that UCHL3 plays a crucial role in the maintenance of stem-like properties and DNA damage repair in several types of cancer[21-26]. Therefore, we proceeded to investigate whether UCHL3 is involved in enhanced stem-like properties and 5-FU chemoresistance due to *TP53* mutation in CRC. In conclusion, our findings suggest that UCHL3 may serve as a potential therapeutic target for reversing high-level glycolysis and enhancing the sensitivity to 5-FU chemotherapy in *TP53*-mutant CRC.

ENO1 has been identified as a multifunctional oncoprotein present both on the cell surface and in the cytoplasm[33]. ENO1 serves as a glycolytic enzyme that catalyzes the conversion of 2-phosphoglycerate to phosphoenolpyruvate, a precursor for pyruvate formation during glycolysis. In the present study, we discovered that UCHL3 exerted its deubiquitinating enzyme activity to stabilize ENO1 protein, which may be responsible for the up-regulation of glycolytic flux and metabolites such as pyruvate by UCHL3 in CRC. Since pyruvate is a master fuel input undergirding citric acid cycle carbon flux, large amounts of pyruvate production caused by UCHL3 may further contribute to oxidative phosphorylation. Additionally, ENO1 has been reported to contribute to stem-like properties and chemotherapy resistance in various cancers, including CRC[34-37]. We also demonstrated that UCHL3 promoted stem-like properties and 5-FU chemoresistance in CRC by stabilizing ENO1. Our results suggest that the aberrant activation of UCHL3−ENO1 axis may be a key driver of elevated glycolysis, enhanced stem-like properties, and 5-FU chemoresistance in *TP53*-mutant CRC.

We screened a library of FDA-approved compounds to identify drugs that significantly suppress UCHL3 expression with the aim of elucidating the mechanism by which *TP53* mutations upregulate UCHL3 expression and repurposing existing drugs to treat *TP53*-mutant CRC. Through our screening, we discovered that Pacritinib significantly inhibited UCHL3 expression by blocking the activation of JAK2−STAT3 pathway in *TP53*-mutant CRC cells. The activation of JAK2−STAT3 pathway is known to enhance tumorigenicity, metastasis, the transformation of CSCs, and chemoresistance in various types of cancer, making it a promising target for the development of anti-tumor agents[38-40]. Previous researches have shown that both p53 inactivation and gain-of-function mutations can activate the JAK2−STAT3 pathway in cancer cells[41,42]. In our study, we found for the first time that the activation of the JAK2−STAT3 pathway induced by *TP53* mutations led to the translocation of phosphorylated STAT3 into the nucleus and its binding to the UCHL3 promoter region, resulting in the upregulation of UCHL3 expression in *TP53*-mutant CRC. Notably, this process could be effectively inhibited by pacritinib treatment.

Previous studies have shown that approximately 80% of *TP53* mutations are missense mutations and about 10% are truncation mutations, which together account for the vast majority of *TP53* mutations[19,43]. Therefore, we focused on the effects of Pacritinib on glycolysis and sensitivity of 5-FU chemotherapy in CRC with *TP53* missense and truncation mutations. Pacritinib was demonstrated to effectively inhibit glycolysis, stem-like properties and enhance the sensitivity of 5-FU chemotherapy in CRC cells with *TP53* missense and truncation mutations *in vitro*. Furthermore, Pacritinib was confirmed to increase the sensitivity of 5-FU chemotherapy in cell line-derived xenograft (CDX) and PDX models with *TP53* missense mutations *in vivo*. The synergistic effects of 5-FU and Pacritinib in the treatment of *TP53*-mutant CRC may be attributed to the fact that DNA damage induced by 5-FU activates mutant p53 proteins, which triggers the JAK2−STAT3−UCHL3−ENO1 axis and thus leads to 5-FU chemoresistance, whereas the combination treatment with pacritinib effectively inhibits the activation of this signaling pathway in *TP53*-mutant CRC. These findings suggest that the combination of pacritinib with 5-FU is particularly recommended for *TP53*-mutant CRC patients, especially those with high UCHL3 expression, to enhance the benefits of chemotherapy. It is worth noting that pacritinib was FDA-approved in February 2022 for the treatment of adults with myelofibrosis[27]. Our study has identified new therapeutic applications for pacritinib in reversing high-level glycolysis and enhancing the sensitivity of 5-FU chemotherapy in *TP53*-mutant CRC. However, further validation through additional clinical trials in the future is still warranted.

5. Conclusions

In conclusion, our study demonstrates that UCHL3 plays a crucial role in high-level glycolysis, enhanced stem-like properties, and

5-FU chemoresistance in *TP53*-mutant CRC by stabilizing ENO1. Notably, we identify a newly FDA-approved drug, Pacritinib, which effectively reverses high-level glycolysis and enhances the sensitivity of 5-FU chemotherapy by blocking the JAK2−STAT3−UCHL3−ENO1 axis in *TP53*-mutant CRC. Our findings propose a novel therapeutic strategy for repurposing pacritinib to improve the prognosis of CRC patients with *TP53* mutations.

Acknowledgements

This study was supported by the National Key Research and Development Program of China (No. 2022YFC3401000 to Zitong Zhao), the National Natural Science Foundation of China (No. 82173332 to Yongmei Song, No. 82272909 to Guiying Wang), the Chinese Academy of Medical Sciences Innovation Fund for Medical Sciences (No. 2023-I2M-2−004 to Yongmei Song, China), the Hebei Province Natural Innovation Group Program (No. H2022206355 to Guiying Wang, China), and the Hebei Province Central Guide Local Science and Technology Special Project (No. 236Z7757G to Guiying Wang, China). We declare that the graphical abstract was created with BioRender.com.

Author contributions

Haisong Xin: Writing − original draft, Validation, Methodology, Investigation, Formal analysis, Data curation. Zitong Zhao: Writing − review & editing, Validation, Methodology, Investigation, Funding acquisition, Data curation. Shichao Guo: Validation, Methodology, Investigation, Formal analysis, Data curation. Ruoxi Tian: Writing − review & editing, Methodology, Formal analysis. Liying Ma: Resources, Methodology, Data curation. Yang Yang: Methodology, Formal analysis. Lianmei Zhao: Methodology. Guanglin Wang: Resources. Baokun Li: Resources. Xuhua Hu: Resources. Yongmei Song: Writing − review & editing, Supervision, Resources, Project administration, Funding acquisition, Conceptualization. Guiying Wang: Writing − review & editing, Supervision, Resources, Funding acquisition, Conceptualization.

Conflicts of interest

The authors have no conflicts of interest to declare.

Appendix A. Supporting information

Supporting information to this article can be found online at https://doi.org/10.1016/j.apsb.2025.03.041.

References

1. Dekker E, Tanis PJ, Vleugels JLA, Kasi PM, Wallace MB. Colorectal cancer. *Lancet* 2019;**394**:1467−80.
2. Brannon AR, Vakiani E, Sylvester BE, Scott SN, McDermott G, Shah RH, et al. Comparative sequencing analysis reveals high genomic concordance between matched primary and metastatic colorectal cancer lesions. *Genome Biol* 2014;**15**:454.
3. Olivier M, Hollstein M, Hainaut P. TP53 mutations in human cancers: origins, consequences, and clinical use. *Cold Spring Harb Perspect Biol* 2010;**2**:a001008.
4. Vousden KH, Prives C. Blinded by the light: the growing complexity of p53. *Cell* 2009;**137**:413−31.
5. Kastenhuber ER, Lowe SW. Putting p53 in context. *Cell* 2017;**170**:1062−78.
6. Zhou YY, Fan XM, Jiao TY, Li WZ, Chen PP, Jiang YM, et al. SIRT6 as a key event linking p53 and NRF2 counteracts APAP-induced hepatotoxicity through inhibiting oxidative stress and promoting hepatocyte proliferation. *Acta Pharm Sin B* 2021;**11**:89−99.
7. Berkers CR, Maddocks OD, Cheung EC, Mor I, Vousden KH. Metabolic regulation by p53 family members. *Cell Metab* 2013;**18**:617−33.
8. Schwartzenberg-Bar-Yoseph F, Armoni M, Karnieli E. The tumor suppressor p53 down-regulates glucose transporters GLUT1 and GLUT4 gene expression. *Cancer Res* 2004;**64**:2627−33.
9. Mantovani F, Collavin L, Del Sal G. Mutant p53 as a guardian of the cancer cell. *Cell Death Differ* 2019;**26**:199−212.
10. Zhang C, Liu J, Liang YJ, Wu R, Zhao YH, Hong XH, et al. Tumour-associated mutant p53 drives the warburg effect. *Nat Commun* 2013;**4**:2935.
11. Liu J, Zhang C, Hu WW, Feng ZH. Tumor suppressor p53 and its mutants in cancer metabolism. *Cancer Lett* 2015;**356**:197−203.
12. Chin KV, Ueda K, Pastan I, Gottesman MM. Modulation of activity of the promoter of the human MDR1 gene by Ras and p53. *Science* 1992;**255**:459−62.
13. Xu J, Wang J, Hu Y, Qian J, Xu B, Chen H, et al. Unequal prognostic potentials of p53 gain-of-function mutations in human cancers associate with drug-metabolizing activity. *Cell Death Dis* 2014;**5**:e1108.
14. Cao X, Hou JY, An QL, Assaraf YG, Wang XD. Towards the overcoming of anticancer drug resistance mediated by p53 mutations. *Drug Resist Updat* 2020;**49**:100671.
15. Shetzer Y, Molchadsky A, Rotter V. Oncogenic mutant p53 gain of function nourishes the vicious cycle of tumor development and cancer stem-cell formation. *Cold Spring Harb Perspect Med* 2016;**6**:a026203.
16. Solomon H, Dinowitz N, Pateras IS, Cooks T, Shetzer Y, Molchadsky A, et al. Mutant p53 gain of function underlies high expression levels of colorectal cancer stem cells markers. *Oncogene* 2018;**37**:1669−84.
17. Garcia-Mayea Y, Mir C, Masson F, Paciucci R, Me LL. Insights into new mechanisms and models of cancer stem cell multidrug resistance. *Semin Cancer Biol* 2020;**60**:166−80.
18. Bykov VJN, Eriksson SE, Bianchi J, Wiman KG. Targeting mutant p53 for efficient cancer therapy. *Nat Rev Cancer* 2018;**18**:89−102.
19. Hassin O, Oren M. Drugging p53 in cancer: one protein, many targets. *Nat Rev Drug Discov* 2023;**22**:127−44.
20. Hafez N, Modather El-Awadly Z, Arafa RK. UCH-L3 structure and function: insights about a promising drug target. *Eur J Med Chem* 2022;**227**:113970.
21. Jerabkova K, Liao YR, Kleiss C, Fournane S, Durik M, Agote-Arán A, et al. Deubiquitylase UCHL3 regulates bi-orientation and segregation of chromosomes during mitosis. *Faseb j* 2020;**34**:12751−67.
22. Song ZW, Tu XY, Zhou Q, Huang JZ, Chen YP, Liu JQ, et al. A novel UCHL3 inhibitor, perifosine, enhances PARP inhibitor cytotoxicity through inhibition of homologous recombination-mediated DNA double strand break repair. *Cell Death Dis* 2019;**10**:398.
23. Liao CY, Beveridge R, Hudson JJR, Parker JD, Chiang SC, Ray S, et al. UCHL3 regulates topoisomerase-induced chromosomal break repair by controlling TDP1 proteostasis. *Cell Rep* 2018;**23**:3352−65.
24. Ouyang LL, Yan B, Liu YT, Mao C, Wang M, Liu N, et al. The deubiquitylase UCHL3 maintains cancer stem-like properties by stabilizing the aryl hydrocarbon receptor. *Signal Transduct Target Ther* 2020;**5**:78.
25. Zhang MH, Zhang HH, Du XH, Gao J, Li C, Shi HR, et al. UCHL3 promotes ovarian cancer progression by stabilizing TRAF2 to activate the NF-κB pathway. *Oncogene* 2020;**39**:322−33.
26. Tang JN, Yang Q, Mao C, Xiao DS, Liu S, Xiao L, et al. The deubiquitinating enzyme UCHL3 promotes anaplastic thyroid cancer progression and metastasis through Hippo signaling pathway. *Cell Death Differ* 2023;**30**:1247−59.
27. Lamb YN. Pacritinib: first approval. *Drugs* 2022;**82**:831−8.
28. Alvarado-Ortiz E, de la Cruz-López KG, Becerril-Rico J, Sarabia-Sánchez MA, Ortiz-Sánchez E, García-Carrancá A. Mutant p53 gain-

of-function: role in cancer development, progression, and therapeutic approaches. *Front Cell Dev Biol* 2020;**8**:607670.
29. Harrigan JA, Jacq X, Martin NM, Jackson SP. Deubiquitylating enzymes and drug discovery: emerging opportunities. *Nat Rev Drug Discov* 2018;**17**:57−78.
30. Fang YZ, Jiang L, He QJ, Cao J, Yang B. Deubiquitination complex platform: a plausible mechanism for regulating the substrate specificity of deubiquitinating enzymes. *Acta Pharm Sin B* 2023;**13**:2955−62.
31. Mennerich D, Kubaichuk K, Kietzmann T. DUBs, hypoxia, and cancer. *Trends Cancer* 2019;**5**:632−53.
32. Ge FJ, Li YK, Yuan T, Wu YL, He QJ, Yang B, et al. Deubiquitinating enzymes: promising targets for drug resistance. *Drug Discov Today* 2022;**27**:2603−13.
33. Qiao G, Wu AG, Chen XL, Tian Y, Lin XK. Enolase 1, a moonlighting protein, as a potential target for cancer treatment. *Int J Biol Sci* 2021; **17**:3981−92.
34. Huang CK, Sun Y, Lv L, Ping Y. ENO1 and cancer. *Mol Ther Oncolytics* 2022;**24**:288−98.
35. Gu JR, Zhong KQ, Wang LG, Ni HS, Zhao YR, Wang XC, et al. ENO1 contributes to 5-fluorouracil resistance in colorectal cancer cells *via* EMT pathway. *Front Oncol* 2022;**12**:1013035.
36. Yang T, Shu X, Zhang HW, Sun LX, Yu L, Liu J, et al. Enolase 1 regulates stem cell-like properties in gastric cancer cells by stimulating glycolysis. *Cell Death Dis* 2020;**11**:870.
37. Shu X, Cao KY, Liu HQ, Yu L, Sun LX, Yang ZH, et al. Alpha-enolase (ENO1), identified as an antigen to monoclonal antibody 12C7, promotes the self-renewal and malignant phenotype of lung cancer stem cells by AMPK/mTOR pathway. *Stem Cell Res Ther* 2021;**12**:119.
38. Jin W. Role of JAK/STAT3 signaling in the regulation of metastasis, the transition of cancer stem cells, and chemoresistance of cancer by epithelial-mesenchymal transition. *Cells* 2020;**9**:217.
39. Yang LQ, Shi PF, Zhao GC, Xu J, Peng W, Zhang JY, et al. Targeting cancer stem cell pathways for cancer therapy. *Signal Transduct Target Ther* 2020;**5**:8.
40. Fu ZW, Wu TT, Gao C, Wang LL, Zhang Y, Shi C. AKR1C1 interacts with STAT3 to increase intracellular glutathione and confers resistance to oxaliplatin in colorectal cancer. *Acta Pharm Sin B* 2024;**14**: 5305−20.
41. Lin J, Tang HJ, Jin XH, Jia GY, Hsieh JT. P53 regulates Stat3 phosphorylation and DNA binding activity in human prostate cancer cells expressing constitutively active Stat3. *Oncogene* 2002;**21**:3082−8.
42. Wörmann SM, Song L, Ai JY, Diakopoulos KN, Kurkowski MU, Görgülü K, et al. Loss of p53 function activates JAK2−STAT3 signaling to promote pancreatic tumor growth, stroma modification, and gemcitabine resistance in mice and is associated with patient survival. *Gastroenterology* 2016;**151**:180−93.e12.
43. Nakayama M, Oshima M. Mutant p53 in colon cancer. *J Mol Cell Biol* 2019;**11**:267−76.